

Molecular Determinants of Potent P2X2 Antagonism Identified by Functional Analysis, Mutagenesis and Homology Docking

Christian Wolf¹, Christiane Rosefort¹, Ghada Fallah, Matthias U. Kassack,
Alexandra Hamacher, Mandy Bodnar, Haihong Wang, Peter Illes, Achim Kless,
Gregor Bahrenberg, Günther Schmalzing, and Ralf Hausmann

Primary Laboratory of origin: Molecular Pharmacology, RWTH Aachen University, 52074

Aachen, Wendlingweg 2, Germany (C.W., C.R., G.F., G.S., R.H.);

Institute of Pharmaceutical & Medicinal Chemistry, Heinrich-Heine-University Düsseldorf,
40225 Düsseldorf, Universitätsstrasse 1, Germany (M.U.K., A.H.); Rudolf-Boehm Institute
for Pharmacology and Toxicology, University of Leipzig, 04107 Leipzig, Härtelstrasse 16-18,
Germany (M.B., H. W., P.I.); Grünenthal GmbH, Global Drug Discovery, Departments of
Molecular Pharmacology and Discovery Informatics, Zieglerstrasse 6, 52078 Aachen,
Germany (A.K., G.B.)

Running title:

Molecular Determinants of Competitive P2X2 Antagonism

Corresponding author:

Ralf Hausmann,

Department of Molecular Pharmacology, University Hospital of RWTH Aachen University,

Wendlingweg 2, D-52074 Aachen, Germany.

Tel +49-241-8089135; Fax +49-241-8082433

E-mail address: rhausmann@ukaachen.de

Number of text pages: 39

Number of figures: 4

Number of tables: 2

Number of supplemental figures: 1

Number of references: 40

Number of words in the Abstract: 236

Number of words in the Introduction: 750

Number of words in the Discussion: 986

Abbreviations used in this manuscript: 2D, two-dimensional; $\alpha\beta$ -meATP, $\alpha\beta$ -methylene-ATP; CI, confidence interval; CNS, central nervous system; Cy5 NHS ester, Cy5 N-hydroxysuccinimide ester; IC₅₀, 50% inhibitory concentration; PPADS, pyridoxalphosphate-6-azophenyl-2',4'-disulfonic acid; TNP-ATP, 2',3'-O-(2,4,6-trinitrophenyl)-ATP; TEVC, two-electrode voltage-clamp; zf, zebrafish.

Abstract

P2X2 receptors are members of the ATP-gated P2X family of cation channels, and they participate in neurotransmission in sympathetic ganglia and interneurons. Here, we identified NF770 as a nanomolar-potent competitive P2X2 receptor antagonist within a series of 139 suramin derivatives. Three structural determinants contributed to the inhibition of P2X2 receptors by NF770: (i) a “large urea” structure with two symmetric phenylenecarbonylimino groups; (ii) attachment of the naphthalene moiety in position 7,7’; and (iii) the specific position of two sulfonic acid groups (3, 3’; 6, 6’) and of one methoxy group (1, 1’) at the naphthalene moiety. This structure–activity relationship was interpreted using a rat P2X2 homology model based on the crystal structure of the closed zebrafish P2X4 receptor. Docking of the suramin derivatives into the modeled ATP-binding pocket provides a uniform explanation for the observed differences in inhibitory potencies. Changes in the chemical structure that increase the inhibitory potency of the suramin derivatives improved the spatial orientation within the ATP-binding pocket to allow for stronger polar interactions of functional groups with Gly72, Glu167 or Arg290. Gly72 is responsible for the orientation of the methoxy group close to Arg290 or Glu167. Combined mutational and functional analysis confirmed that residues Gly72 and Glu167 are as important for ATP binding as Arg290, whose ATP-binding role has been shown in previous studies. The *in silico* prediction of Gly72 and Glu167 as ATP-binding residues strongly supports the validity of our homology docking.

Introduction

P2X receptors, a family of ion channels that are gated by extracellular ATP, are homotrimers and heterotrimers (Aschrafi et al., 2004; Nicke et al., 1998) assembled from a repertoire of seven homologous subunits, P2X1–P2X7 (Burnstock, 2004). P2X receptors are expressed on the surface of a large variety of excitable and non-excitable cell types and are involved in numerous processes, including sensory neurotransmission, platelet aggregation, smooth muscle contraction, immune responses and inflammation (Burnstock, 2008; Finger et al., 2005; Gever et al., 2006; Jarvis and Khakh, 2009; Surprenant and North, 2009). There is strong evidence that at least four P2X receptor subtypes play a role in nociception, including homomeric P2X3, P2X4 and P2X7 receptors and the heteromeric P2X2/3 receptor (Burnstock, 2008; Surprenant and North, 2009).

Several P2X receptor antagonists have been developed to target pain and inflammation. A-317491, a selective dual inhibitor of P2X3 and P2X2/3 receptors, has strong antinociceptive effects in rodents (Jarvis et al., 2002), but it has not been developed further due to its poor distribution into the central nervous system (CNS) (Gever et al., 2006). Selective dual inhibition of P2X3 and P2X2/3 receptors has also been achieved by the diaminopyrimidine derivatives RO-3, RO-4 and RO-51 (Gever et al., 2010; Jahangir et al., 2009; Jarvis and Khakh, 2009). Among these, RO-3 and RO-4 (recently redesignated AF-353) distribute well into tissues, including the CNS, and exert beneficial effects in rodent models of pain and models of bladder function (Gever et al., 2006; Gever et al., 2010; Jarvis, 2010). RO-85, the first orally bioavailable drug-like P2X3 receptor antagonist, is selective for P2X3 receptors over P2X2/3 and other P2X receptor subtypes. RO-85 inhibits rat and human P2X3 receptors with pIC_{50} values of 7.5 and 6.4, respectively, and is only weakly potent ($\text{pIC}_{50} < 5$) at non-P2X3 receptor subtypes, including the human P2X2/3 receptor (Brotherton-Pleiss et al., 2010). The newly developed P2X7 receptor-selective antagonists GSK314181A, A-

740003, A-438079, A-839977 and A-804598 also have analgesic effects in rodent models of pain (for review see (Jarvis, 2010)).

The reduced nociceptive signaling seen in P2X2 knock-out mice during the persistent phase of the formalin model of pain seems to result from reduced signaling through heteromeric P2X2/3 channels rather than from homomeric P2X2 receptors (Cockayne et al., 2005). In several acute pain models, however, P2X2-containing receptors (homomeric P2X2 and heteromeric P2X2/3 receptors) are not critical for acute nociceptive responses (Cockayne et al., 2005). By contrast, homomeric P2X2 receptors facilitate excitatory transmission onto interneurons (Khakh et al., 2003) and play pivotal roles in the mediation of neuronal ventilatory responses (Rong et al., 2003) and in sympathetic autonomous neurotransmission (Cockayne et al., 2005). P2X2/3 heteromeric receptors are also involved in the transmission of sensory information from taste buds, but they are less important than P2X3 receptors in this pathway (Finger et al., 2005). Pharmacological experiments evaluating the role of homomeric P2X2 receptors in these processes are impeded by the lack of selective agonists and potent antagonists (Burnstock, 2008; Jarvis and Khakh, 2009). Current P2X receptor antagonists are non-selective and have, at best, micromolar potencies for P2X2 receptors (Gever et al., 2006; Jarvis and Khakh, 2009). PPADS, for instance, blocks homomeric P2X1, P2X2 and P2X3 receptors with a similar IC_{50} of $\sim 1 \mu M$ (Gever et al., 2006; Jarvis and Khakh, 2009). TNP-ATP blocks P2X1, P2X2/3 and P2X3 receptors with nanomolar potency, but it is 1000-fold less potent in blocking homomeric P2X2 receptors (Gever et al., 2006; Jarvis and Khakh, 2009). We have previously identified the suramin derivatives NF449 and NF110 as potent antagonists of P2X1 and P2X3 receptors, respectively (Hausmann et al., 2006; Kassack et al., 2004; Rettinger et al., 2005). Suramin itself non-selectively inhibits P2X2 receptors with a potency similar to that of PPADS or TNP-ATP (Jarvis and Khakh, 2009; Trujillo et al., 2006). Consequently, we screened a series of 139 suramin derivatives and identified NF770 as a

P2X2 receptor antagonist with nanomolar potency and selectivity over P2X1, P2X4 and P2X7 receptors.

The 3.0-Å-resolution X-ray structure of the closed-state zebrafish (zf) P2X4 receptor (Kawate et al., 2009) enables homology modeling of other P2X receptor family members for rational ligand design (Jarvis, 2010) and facilitated mutagenesis-based studies of structural rearrangements that accompany channel opening (Cao et al., 2009;Jiang et al., 2010;Keceli and Kubo, 2009;Kracun et al., 2010). For a molecular interpretation of the observed structure–activity relationships, we generated a closed-state homology model for rat P2X2 (rP2X2) using the zfP2X4.1 structure (Kawate et al., 2009) as template and performed *in silico* docking experiments that resulted in the identification of the molecular determinants of P2X2 antagonism and two novel amino acid residues important for ligand binding.

Materials and Methods

Chemicals

A diverse library of suramin derivatives available from previous studies was synthesized according to published methods (Kassack et al., 2004;Ullmann et al., 2005). The chemical structures of the suramin derivatives studied in greater detail are shown in Table 2. Stock solutions (10 mM) were prepared in water and stored at -20°C until the day of the experiment. All other chemicals were purchased from either Sigma-Aldrich (Taufkirchen, Germany) or Merck (Darmstadt, Germany) in the highest available quality.

P2X receptor expression in X. laevis oocytes

Oocyte expression plasmids encoding wild-type and hexahistidyl-tagged rat P2X subunits (rP2X1, rP2X2, rP2X3, rP2X4, rP2X7) from previous studies were used (Aschrafi et al., 2004;Hausmann et al., 2006;Nicke et al., 1998). Chimeric constructs for rP2X2¹⁻⁴⁷X1⁴⁸⁻³⁹⁹ and rP2X2¹⁻⁴⁷X3⁴²⁻³⁹⁷ encoding amino acids Met¹-Val⁴⁷ of the rP2X2 subunit joined in frame with ⁴⁸Val-³⁹⁹Ser of the rP2X1 subunit or ⁴²Val-³⁹⁷His of the rP2X3 subunit, respectively, have also been described previously (Hausmann et al., 2006). Replacement mutations (G⁷²A-rP2X2, R²⁹⁰A-rP2X2) were introduced with QuikChange site directed-mutagenesis (Stratagene, La Jolla, CA). All constructs were verified with restriction analysis and nucleotide sequencing. Capped cRNAs were synthesized as described previously (Nicke et al., 1998) and injected into collagenase-defolliculated *X. laevis* oocytes in aliquots of 41 nl (wild-type) or 23 nl (chimeras rP2X2-X1 and rP2X2-X3) using a Nanoliter 2000 injector (WPI, Sarasota, FL, USA). To express the heteromeric rP2X2/3 receptor, rP2X2 and rP2X3 cRNA were co-injected at a 1:2 ratio (w/w). Oocytes were cultured at 19°C in sterile oocyte Ringer's solution (ORi: 90 mM NaCl, 1 mM KCl, 1 mM CaCl₂, 1 mM MgCl₂, and 10 mM HEPES, pH 7.4) supplemented with 50 µg/ml of gentamicin.

Two-electrode voltage-clamp electrophysiology

One to three days after cRNA injection, current responses were evoked with ATP or $\alpha\beta$ -meATP at ambient temperature (21–24°C) in the absence or presence of suramin derivatives and recorded with conventional two-electrode voltage-clamp (TEVC) with a Turbo TEC-05 amplifier (npi Electronics, Tamm, Germany) at a holding potential of –60 mV, as described previously (Hausmann et al., 2006). On the day of the experiment, agonists and suramin derivatives were diluted from the frozen aqueous stock solutions. Oocytes were continuously perfused by gravity flow (5–10 ml/min) in a small flow-through chamber (volume ~10 μ l) with a nominally calcium-free ORi solution (designated Mg-ORi), in which CaCl_2 was replaced with equimolar MgCl_2 to avoid a contribution of endogenous Ca^{2+} -dependent chloride channels to the agonist response. To record rP2X7 receptor-mediated currents, a bathing solution consisting of 94 mM NaCl, 1 mM KCl, 0.1 mM flufenamic acid, and 10 mM HEPES-NaOH, pH 7.4 was used (Becker et al., 2008; Hausmann et al., 2006). Switching between bath solutions was controlled by a set of computer-operated magnetic valves controlled by the CellWorks E 5.1 software (npi Electronics, Tamm, Germany). When analyzing the inhibitory effects, the following agonist concentrations were used: 100 μ M ATP for rP2X7, 10 μ M ATP for rP2X2 and rP2X4, 1 μ M ATP for rP2X1 and rP2X3, 10 nM ATP for rP2X2-X1 and rP2X2-X3 chimeras, and 1 μ M $\alpha\beta$ -meATP for rP2X2/3 (Hausmann et al., 2006). The application of agonists and antagonists was tailored to fit the specific experimental needs of each P2X receptor based on the presence or absence of desensitization, as reported previously (Hausmann et al., 2006). Representative current traces from the non-desensitizing rP2X2 receptor and the fast-desensitizing rP2X1 receptor are shown in Figure 1.

Protein labeling, purification, and PAGE

cRNA-injected oocytes were metabolically labeled by overnight incubation with [^{35}S]-methionine. Immediately before protein extraction, the oocytes were additionally surface-

labeled with Cy5 NHS ester, an amine-reactive, membrane-impermeant fluorescent dye, as described previously (Becker et al., 2008). His-tagged proteins were purified by Ni-NTA agarose (Qiagen) chromatography from digitonin (1% w/v) extracts and analyzed with blue native PAGE (BN-PAGE), as described previously (Aschrafi et al., 2004; Nicke et al., 1998). The migration positions of P2X2 dimers and monomers were determined by co-analyzing the partially denatured P2X2 receptor. This was achieved by treating the samples for 1 h at 37°C with 0.1% (w/v) SDS or a combination of 0.1% (w/v) SDS and 100 mM DTT before BN-PAGE.

For SDS-urea-PAGE, proteins were denatured by incubation with a reducing SDS sample buffer for 15 min at 56°C and electrophoresed in parallel with ¹⁴C-labeled molecular mass markers (Rainbow, Amersham) on SDS-urea gels with 10% acrylamide. After electrophoresis, gels were scanned wet with a fluorescence scanner (Typhoon, GE Healthcare) to visualize the fluorescently labeled plasma membrane-bound proteins and then dried and exposed to a phosphor screen for subsequent analysis using the PhosphorImager (Storm 820, GE Healthcare) to detect ³⁵S incorporation. Figures were prepared with ImageQuant TL v2005 (Amersham) for contrast adjustments and Adobe Photoshop CS 4 for level adjustment and cropping.

Data analysis

Data were plotted and fitted using Prism5 (GraphPAD Software Inc., San Diego, CA). Agonist concentration–response values were generated by normalizing the current amplitudes to the control response induced by a supermaximally effective ATP concentration of 1 mM. Agonist concentration–response curves and EC₅₀ values were obtained by iteratively fitting the Hill equation (Eq. 1) to the normalized data points from 5–11 oocytes.

$$I/I_{\max} = 1 / \left(1 + ([EC_{50}/A])^{n_H} \right) \quad (\text{Eq. 1})$$

where I is the current evoked by agonist concentration A , I_{\max} is the maximal current response and n_H is the Hill coefficient.

Antagonist concentration–response values were generated by normalizing the ATP-induced current amplitudes in the presence of the antagonist to the control response in the absence of the antagonist. Concentration–inhibition curves and IC_{50} values were derived from the non-linear least-squares fit (Eq. 2) of the pooled data points.

$$I_{\text{Ant}}/I_{\max} = 1 / \left(1 + ([\text{Ant}]/IC_{50})^{n_H} \right) \quad (\text{Eq. 2})$$

where I_{\max} is the control response in the absence of antagonist (Ant), I_{Ant} is the current response at the respective antagonist concentration, and IC_{50} is the antagonist concentration that causes 50% inhibition of the current elicited by a given agonist concentration.

EC_{50} and IC_{50} values are presented as the geometric means and their 95% confidence intervals. Mean current amplitudes, Hill slopes and other values are presented as arithmetic means \pm SEM. Error bars were omitted in the figures when they were smaller than the symbols used.

Homology Model of the rP2X2

We used the standard modeling techniques implemented in MOE2008.10 (Molecular Operating Environment 2008, Chemical Computing Group: 1010 Sherbrooke Street West, Suite 910, Montreal Que., Canada H3A 2R7) to generate a homology model of the rP2X2 receptor based on the X-ray structure of zebrafish P2X4 (Kawate et al., 2009). The entry 3H9V from the Protein Data Bank was used as a template, which is believed to represent the closed state of the channel. The sequence of rP2X2 was retrieved from accession number P49653 of the UniProtKB database. Sequence alignment between the template and the model sequence was performed using a modified version of the alignment algorithm originally introduced by Needleman and Wunsch (Needleman and Wunsch, 1970). In this approach,

alignments are computed by optimizing a function based on residue similarity scores. The function uses the amino acid substitution matrix BLOSUM62 (Henikoff and Henikoff, 1992) and gap penalties and was constrained, in this case, by the 10 known conserved extracellular cysteine residues, which were adjusted and fixed manually. The presented homology model is based on the best scoring of 25 generated intermediate models and the overall structural quality confirmed by a Ramachandran plot. The intermediate homology models were refined with the Amber89 force field (Summa and Levitt, 2007) using a fine gradient, which was terminated when the root mean square was $< 1 \text{ \AA}$. The electrostatic solvation energy was used to score the 25 models; it was calculated using a generalized born/volume integral method (Labute, 2008). The protonation of the final model was done using the Protonate3D algorithm followed by minimization with a root mean square of 0.5 \AA (Labute, 2009). This homology model was used for the docking procedure (Fig. 3). The lowest energy conformations of the suramin derivatives (NF742, NF769, NF770, NF778) were deprotonated to sulfonates, as they exist at physiological pH. The receptor model was kept rigid during the docking computation, whereas the suramin derivatives were allowed to remain flexible, permitting possible bond rotations.

Results

Three (out of 139) suramin analogs exhibit nanomolar potency at the rP2X2 receptor

At 10 μ M ATP, suramin inhibited the oocyte-expressed rP2X2 receptor with an IC_{50} value of 0.49 μ M. This value is at the bottom of the range of published IC_{50} values (1–34 μ M; (Gever et al., 2006)). In contrast, our EC_{50} value for ATP of 21.8 (17.4–23.2) μ M was in the range reported by others (Jiang et al., 2010). The unexpectedly potent inhibition of the rP2X2 receptor by suramin prompted us to screen an available library of 139 suramin derivatives synthesized according to methods published previously (Kassack et al., 2004; Ullmann et al., 2005). To accelerate TEVC screening, we arranged 1 μ M aqueous solutions of 139 suramin derivatives in two sets of matrices, A and B, comprising 81 and 58 derivatives, respectively. Equal aliquots from each horizontal row were combined to yield row mixtures of nine or six to seven suramin derivatives. Likewise, equal aliquots from each vertical column were combined to yield column mixtures of nine or, in one case, four suramin derivatives. Accordingly, each compound was present in two mixtures: one row and one column mixture. With a total of 34 TEVC measurements representing 18 rows and 16 columns, we could identify four row mixtures and three column mixtures that inhibited the rP2X2 receptor-mediated currents by >75%. By determining the intersection of active row and column mixtures, seven putatively active suramin derivatives were identified: NF127, NF708, NF710, NF739, NF770, NF776 and NF778. Individual testing showed that at 1 μ M, NF708, NF710, NF127, and NF739 inhibited the ATP-gated rP2X2 receptor currents by 18%, 7%, 39%, and 14%, respectively, and they were not tested further at the other P2X receptor isoforms. In contrast, NF770, NF776 and NF778, at 1 μ M each, inhibited the ATP-gated rP2X2 receptor currents by 84–96% and were characterized in detail.

Concentration–response analysis of NF770, NF776 and NF778 at different P2X receptor subtypes

To determine the P2X receptor subtype selectivity of the three most potent rP2X2 receptor–blocking suramin derivatives (NF770, NF776 and NF778), concentration–response curves were generated for the rP2X1, rP2X2, rP2X2/3, rP2X3, rP2X4 and rP2X7 receptors (Fig. 1C-E). The P2X5 receptor was not studied because in humans, the P2X5 subunit occurs predominantly as an assembly-deficient natural deletion mutant that lacks much of the TM2 and pre-TM2 regions as a result of the splicing out of exon 10 (Duckwitz et al., 2006). The P2X6 receptor was also omitted because P2X6 does not form functional homomeric channels under most circumstances (Gever et al., 2006). ATP elicited non-desensitizing currents in wt-rP2X2 and wt-rP2X2/3 receptors. This allowed for the steady-state analysis of drug-induced current inhibition as a visible decline of the current amplitude to a new plateau (see current traces in Fig. 1A). In contrast, wt-rP2X1 and wt-rP2X3 receptors desensitized rapidly in the continued presence of agonist (see current traces in Fig. 1B). If agonist and antagonist bind to the same receptor with different rate constants, the current transient is too short to allow a binding equilibrium to be reached between the co-applied compounds (Hausmann et al., 2006). To assess the inhibition of P2X1 and P2X3 receptors under steady-state conditions, non-desensitizing rP2X2-X1 and rP2X2-X3 receptor chimeras were used, in which the N-terminal tail, including the first transmembrane domain, are replaced by the complementary portion of the rP2X2 subunit (Hausmann et al., 2006). Because the ligand-binding ectodomain originates entirely from the rP2X1 or the rP2X3 subunit, these chimeras can be reliably used as non-desensitizing substitutes of wt-rP2X1 and rP2X3 receptors. While ATP served as an agonist for all the above receptors, the non-desensitizing heteromeric rP2X2/3 receptor was selectively activated by 1 μ M α,β -meATP to avoid activation of the co-expressed homomeric rP2X2 receptor, which responds to ATP but virtually not to $\alpha\beta$ -meATP (Gever et al., 2006).

Concentration–inhibition curves and IC₅₀ values were derived from non-linear least-squares fits of the Hill equation to the pooled data points. The following rank order of potencies was determined for NF770 (Fig. 1C, Table 1): wt-rP2X2 \geq rP2X2-X3 > wt-rP2X2/3

> wt-rP2X3 > rP2X2-X1 > wt-rP2X1 > > wt-rP2X4, wt-rP2X7. A similar rank order was obtained for NF776 and NF778, except that the positions of rP2X1 and rP2X3 were reversed (Fig. 1D,E and Table 1). All three suramin derivatives were almost ineffective in blocking rP2X4 or rP2X7 receptor-mediated currents (<10% inhibition at 10 μ M for either suramin derivative; data not shown).

NF770 inhibits the rP2X2 receptor competitively

To delineate whether NF770 acts as a competitive antagonist of the P2X2 receptor, ATP concentration–response curves were established in the absence and presence of NF770. Representative current traces recorded at distinct concentrations of NF770 are shown in Fig. 2A. In this experimental series, ATP activated rP2X2 receptor-mediated inward currents with an EC₅₀ value of 20.7 μ M. Increasing concentrations of NF770 progressively shifted the ATP concentration–response curves parallel to the right without changing the maximal response (Fig. 2B). Linear regression analysis of Schild plot data (Fig. 2C) yielded a correlation coefficient of 0.996, a slope of 0.74 ± 0.03 , and an abscissa intercept of -6.96, corresponding to a pA₂ value of 6.96. Altogether, these data strongly indicate that NF770 and ATP interact competitively at the rP2X2 receptor.

Structure–activity relationships of suramin derivatives as P2X2 receptor antagonists

To identify the structural determinants of P2X2 receptor inhibition, we established concentration–response relationships for compounds that are more closely related to either suramin (compound 2) or to NF770 (compound 15) in terms of the number of sulfonic acid groups or the presence of a methoxy group, respectively. The chemical structures of these compounds and their IC₅₀ values at the rP2X2 receptor are shown in Table 2. Large urea derivatives contained two symmetric phenylenecarbonylimino groups linking the urea backbone with the naphthalene moieties (Table 2, compounds 1–3 and 13–16). Small urea

derivatives contained only one symmetric phenylenecarbonylimino group between the urea backbone and the naphthalene moieties (Table 2, compounds 4–12).

Replacing the methyl substituent of the phenylene ring of suramin with hydrogen (compound 1) or ethyl (compound 3) had virtually no effect on the inhibitory potency (IC_{50} 0.28–0.49 μ M). The corresponding small urea derivatives i.e., (compounds 4–6), were 30–46-fold less potent in inhibiting the rP2X₂ receptor (IC_{50} 9.9–14.4 μ M). The potency declined further when the position of one of the sulfonic acid groups was changed from the *para* to the *meta* position relative to the amino group (cf. compounds 5 and 7). In contrast, replacement of the sulfonic acid group in position 1 by a methoxy group in the small urea backbone increased the inhibitory potency ~4-fold when the positions of the two remaining sulfonic acid groups were left unchanged (cf. compounds 7 and 8) and ~2-fold when the two remaining sulfonic acid groups were differently positioned (cf. compounds 7 and 9).

An increase in the inhibitory potency of the trisulfonic acid derivatives also occurred when the position of the naphthalene moiety relative to the amino group was changed from position 8,8' (α -aminonaphthalene, compounds 4-7) to position 7,7' (β -aminonaphthalene, compound 10). Combining the replacement of one sulfonic acid group by a methoxy group and replacing the α -aminonaphthalene by a β -aminonaphthalene (corresponding to position 7,7' in compound 15 (NF770) and to position 6,6' in compound 12 (NF776)) increased the inhibitory potency further (cf. compounds 10 and 11 or 12). The resulting compound, NF776 (compound 12), was the most potent rP2X₂ receptor blocker in this series of small urea derivatives.

Next, we examined whether similar beneficial effects could also be realized in the context of large urea derivatives. We observed a ~34-fold increase of the inhibitory potency of the 8,8' aminonaphthalene derivatives by changing the position of the methoxy group at the naphthalene moiety from position 1 to 3 (cf. compound 13 and 14). An even larger (>1000-fold) increase occurred when the α -aminonaphthalene moiety was replaced by a β -

aminonaphthalene (from the 8,8' (compound 13) to the 7,7' position (compound 15)), thus yielding the most potent rP2X2 receptor–blocking suramin derivative in this study, NF770. The solely available α -aminonaphthalene derivative with positionally different sulfonic acid and methoxy groups, NF778 (compound 16), was 7-fold less potent than NF770 (compound 15), again indicating the importance of the position of the methoxy group.

Molecular docking of suramin derivatives on a homology-modeled rP2X2 receptor

The above results identified three structural determinants of suramin derivatives that contribute to efficient P2X2 receptor inhibition: (i) a “large urea” structure with two symmetric phenylenecarbonylimino groups linking the urea backbone with the naphthalene moiety, (ii) substitution of one of the three sulfonic acid groups by a methoxy group, and (iii) using a β -aminonaphthalene moiety rather than a α -aminonaphthalene. To assign these chemical structure determinants to molecular features of the rP2X2 ATP-binding pocket, we generated a homology model of the rP2X2 receptor using the zfP2X4 receptor X-ray structure as a template. Because the zfP2X4 receptor structure has been solved in the absence of bound ATP, the exact location of the ATP-binding pocket is unknown. However, by interpreting the zfP2X4 receptor structure in the context of functional mutagenesis data, it has been inferred that each of the three ATP-binding pockets per homotrimer is represented by a deep groove on the outside of the protein that is assembled from two complementary half-shells provided by two adjacent subunits (Kawate et al., 2009). A corresponding groove is also present in our P2X2 homology model and includes several basic residues (Lys⁶⁹, Lys⁷¹, Lys³⁰⁸) and the ²⁸⁸NFR²⁹⁰ motif (Fig. 3A), which have all been implicated in ATP binding (Ennion et al., 2000; Fischer et al., 2007; Guerlet et al., 2008; Roberts et al., 2008; Roberts and Evans, 2004).

We selected a set of four suramin derivatives (NF742, NF769, NF770, and NF778) that were representative of the structural hallmarks described above. Our docking experiments revealed that the hydrophilic cavity formed between two adjacent subunits of the homotrimer,

presumed to represent the ATP-binding site, was large enough to accommodate any of the four suramin derivatives, including the large urea derivative NF770 (Fig. 3A). The perfect fit enabled the NF770 molecule to interact with residues both deep in the ATP-binding pocket and in the outer sphere (Fig. 3A). The interactions of NF770 are summarized in a two-dimensional (2D) ligand plot (Fig. 3C) that shows the Gaussian contact surfaces within a radius of 4.5 Å around the atoms of the ligands. Corresponding 2D ligand plots of NF769, NF742 and NF778 are shown in (Supplemental Figure 1A-C).

We then determined which amino acid residues are involved in ligand binding without explicitly determining the differing binding energies of the four compounds. We identified three residues, Lys279, Lys246 and Lys71, that formed hydrogen bonds with the acidic groups of the suramin derivatives (Fig. 3B,C and Supplemental Figure 1A-D) in a manner similar to that suggested for the interaction with the phosphate oxygens of ATP (Roberts et al., 2008; Wilkinson et al., 2006).

The most important differences in the binding modes, which determine the binding energy and the block of ATP function, resulted from the differences in the interactions with residues Gly72, Arg290 and/or Glu167. While NF778 interacted with Gly72 and Glu167 (Supplemental Figure 1C,D), NF770 and NF769 interacted with Gly72 and Arg290 (Fig. 3B). In contrast, the 20–1000-fold less potent NF742 did not interact with any of these residues (Fig. 3B). Moreover, NF742 was incapable of forming a potency-determining interaction with residues other than Lys71, Lys246 and Lys279, which contribute equal binding energies for all the compounds (see above). Therefore, NF742 cannot block ATP binding as potently as NF769, NF770 or NF778.

In our model, the oxygen of the methoxy group of NF770 is 2.1 Å from Arg290 (acceptor-hydrogen distance), thus enabling the formation of a strong, direct hydrogen bond, which contributes crucially to the free binding enthalpy and is essential for blocking the ATP from binding. In the less potent small urea NF769, the methoxy group and Arg290 are ~3.7 Å

apart. This interaction may be mediated by a bridging water molecule, which weakens the electrostatic effect with regard to the binding energy and steric hindrance for ATP binding.

Comparing NF770 and NF778, which differ only in the positions of the sulfonic acid and methoxy groups at the naphthalene moiety, shows different interaction modes in our homology model-based docking experiments (Supplemental Figure 1C,D). The strong hydrogen bond-based interaction of NF770 with Arg290 that crucially determines the binding energy is replaced in NF778 by a weaker interaction of the methoxy group with the backbone of Glu167 (Supplemental Figure 1C,D). This is due to the different substitution pattern of NF778 (1-methoxy-3,5-disulfonic acid) compared to NF770 (1-methoxy-3,6-disulfonic acid). In addition, the intraligand spatial orientation of the functional groups is important for the fixation of the ligand conformation. This is apparent, for instance, from a comparison of the 7,7' and 8,8' aminonaphthalene derivatives, which shows that the position of the naphthalene linkage affects the distance of the methoxy group to the amide moiety. A larger distance, such as the one in the 7,7'-aminonaphthalene derivatives NF769 and NF770, enhances the flexibility of the linkage and allows for a better fit within the ligand-binding pocket and tighter ligand binding.

Contribution of Gly72 and Glu167 to ATP potency

While the role of Arg290 in ATP binding to P2X2 receptors is already well documented (Guerlet et al., 2008; Roberts et al., 2008), a contribution of Gly72 and Glu167 has not been observed previously. To functionally verify the importance of these residues for ATP binding, we expressed single point mutants of the rP2X2 receptor in *X. laevis* oocytes and recorded the ATP-gated cation currents with TEVC. ATP concentration-response analysis of the G⁷²A-rP2X2 receptor revealed a ~3-fold decrease in the maximal current amplitudes and a >13-fold increase in the EC₅₀ value from 18.5 (14.5-23.6) μ M (Fig. 4B, wild-type) to 244 (212-271) μ M (Fig. 4B, G⁷²A mutant). The E¹⁶⁷A-rP2X2 receptor exhibited virtually identical maximal

current amplitudes but a ~5-fold decrease in the EC_{50} value compared to the wt-rP2X2 receptor (Fig. 4B). The current shape (Fig. 4A), trimeric assembly (data not shown) and cell surface expression of both the G⁷²A and the E¹⁶⁷A mutant P2X2 receptor were unaffected compared to the wt-rP2X2 receptor (Fig. 4C). Mutant Arg290, corresponding to Arg298 in zfP2X4, was analyzed as a positive control. Consistent with its crucial role in ATP binding (Guerlet et al., 2008; Kawate et al., 2009; Roberts et al., 2008), the R²⁹⁰A mutation resulted in an ~16-fold decrease in the maximal current amplitudes and a 27-fold increase in the EC_{50} value compared to the wt-rP2X2 receptor (Fig. 4B). The current shape (Fig. 4A), trimeric assembly (data not shown) and cell surface expression (Fig. 4C) were unchanged. These data indicate that ATP binding is crucially determined by the same amino acid residues that were identified by homology modeling to determine the potency of suramin derivatives at the rP2X2 receptor.

Discussion

NF770 is a nanomolar-potent P2X2 receptor antagonist

We used TEVC to show that the divalent suramin analogue NF770 competitively inhibits recombinant P2X2 receptor subtypes expressed in *Xenopus* oocytes with an IC₅₀ value of 19 nM. To the best of our knowledge, NF770 represents the most potent rP2X2 receptor antagonist described so far. At the other P2X receptors, NF770 exhibits the following rank order of potencies based on IC₅₀ values: wt-rP2X2 ≥ rP2X2-X3 ≥ wt-rP2X2/3 > wt-rP2X3 > rP2X2-X1 > wt-rP2X1 > > wt-rP2X4, wt-rP2X7.

NF770 is >50-fold more potent than the P2X antagonists that are currently regarded to be the most potent for the rP2X2 receptor: suramin, PPADS and TNP-ATP. In addition, NF770 exhibits a ~10-fold selectivity for the P2X2 receptor over the P2X1 receptor. This suggests that NF770 has an advantageous profile compared to presently known compounds, which are non-selective with regard to P2X1 and P2X3 receptors (suramin and PPADS) or much more potent at the P2X1 and P2X3 receptor than at the P2X2 receptor (TNP-ATP) (Gever et al., 2006; Jarvis and Khakh, 2009). However, it is unclear so far whether NF770 will inhibit the rP2X2 receptor in functional assays with the same high potency as on *X. laevis* oocytes. With the rP2X1 receptor-selective suramin derivatives NF449 and NF279, for instance, we observed a markedly reduced potency in the isolated rat vas deferens as compared to the oocyte-expressed rP2X1 receptor (Braun et al., 2001). Also, the selectivity profile towards other receptors than P2X receptors has not yet been determined and therefore effects mediated by other functionally important proteins in native tissues cannot be excluded.

The inhibitory potency of suramin derivatives is crucially determined by strong polar interactions within the ATP-binding pocket

Using structure–activity relationship analysis, we identified three structural determinants that contribute to efficient, competitive P2X2 receptor inhibition by suramin derivatives: (i) a

“large urea” structure with two symmetric phenylenecarbonylimino groups linking the urea backbone with the naphthalene moiety, (ii) using a β -aminonaphthalene moiety rather than a α -aminonaphthalene, and (iii) the positioning of two sulfonic acid groups and a monomethoxy group at the naphthalene moiety. Our homology modeling–based ligand docking provides a uniform explanation of these findings. All of the changes to the chemical structures that increase the potency of the suramin derivatives at the rP2X₂ receptor improve the spatial orientation within the ATP-binding pocket to allow for stronger polar interactions of functional groups (sulfonic acids or methoxy groups) with the amino acid residues important for ATP binding. First, the addition of a central phenylenecarbonylimino moiety reduces the acceptor-hydrogen distance between the oxygen of the methoxy group of NF770 and Arg290 from 3.7 to 2.1 Å, enabling the formation of a strong, direct hydrogen bond, which crucially determines the binding energy. Second, using a β -aminonaphthalene moiety rather than a α -aminonaphthalene places the methoxy group closer to the polar amino acid residues of the binding pocket (Arg290 and Glu167), resulting in an increase of the inhibitory potency at the rP2X₂ receptor. Third, the different positions of the polar substituents at the naphthalene moiety affect the interaction modes within the ATP-binding site. In NF770, the interaction of one of the two sulfonic acid groups with Gly72 places the methoxy group in an orientation that enables it to form a strong hydrogen bond with Arg290. In NF778, only a weaker interaction with the backbone of Glu167 is feasible, thus explaining its ~7-fold potency compared to NF770.

Finally, also interligand interactions contribute to ligand potency. Certain positions of the naphthalene linkage and the substituents at the naphthalene moiety favor a closer proximity of the amide linker with the polar substituents. As a consequence, the free rotatability of the naphthalene moiety at the amide linker is significantly reduced, resulting in a partial conformational fixation that hinders the optimal fitting of the ligand into the binding pocket.

Homology docking identifies two novel P2X2 receptor residues involved in ATP binding

Our homology docking assigned for the first time to the residues Gly72 and Glu167 a role in ligand binding. This finding was verified functionally with single alanine substitutions of Gly72 and Glu167 that resulted in marked changes in ATP potency and, in the case of Gly72, in the maximum current amplitude. Indirectly, these data strongly support the versatility of our homology model of the rP2X2 receptor, particularly for the presumed ATP-binding pocket.

We suggest that Gly72, Glu167 and Arg290 are directly involved in ligand binding rather than in channel gating. First, corresponding residues of the zfP2X4 receptor are all located within the suggested ATP-binding site, and Arg290 of rP2X2 and corresponding residues of other P2X isoforms have been unequivocally shown to participate in ATP binding (Ennion et al., 2000;Fischer et al., 2007;Guerlet et al., 2008;Roberts et al., 2008;Roberts and Evans, 2004). Second, recently the pore region and the channel gate have been assigned to pre-TM and TM2 residues (Cao et al., 2009;Jiang et al., 2010;Keceli and Kubo, 2009;Kracun et al., 2010). In addition to Arg290, Lys69, Lys71 and Lys308 (numbered according to the rP2X2 subunit), several phenylalanine and threonine residues are involved in the binding of ATP to P2X receptors, including P2X2 (Guerlet et al., 2008;Roberts et al., 2008), P2X1 (Ennion et al., 2000;Roberts and Evans, 2004) and P2X3 (Fischer et al., 2007). To the best of our knowledge, our work is the first to demonstrate that Gly72 and Glu167 are potency-determining residues for competitive P2X2 receptor antagonism and are crucially involved in ATP binding. A similar role in ligand binding is also true for Arg290, which has already been identified in previous studies to be involved in ATP binding (Ennion et al., 2000;Fischer et al., 2007;Guerlet et al., 2008;Roberts et al., 2008;Roberts and Evans, 2004).

The identification of Gly72-driven ligand orientation inside of the binding pocket is of significant interest for molecular ligand design or lead optimization.

Acknowledgments

We thank Ursula Braam for expert technical assistance in the molecular biology experiments.

Authorship Contributions

Participated in research design: Schmalzing, Hausmann, Bahrenberg, Kless.

Conducted experiments: Wolf, Rosefort, Fallah, Bodnar, Wang, Kless.

Contributed new reagents or analytic tools: Hamacher, Kassack.

Performed data analysis: Hausmann, Illes, Kless, Bahrenberg.

Wrote or contributed to the writing of the manuscript: Schmalzing, Hausmann.

Other: Schmalzing and Hausmann acquired funding for the research.

References

- Aschrafi A, Sadtler S, Niculescu C, Rettinger J and Schmalzing G (2004) Trimeric Architecture of Homomeric P2X2 and Heteromeric P2X1+2 Receptor Subtypes. *J Mol Biol* **342**:333-343.
- Becker D, Woltersdorf R, Boldt W, Schmitz S, Braam U, Schmalzing G and Markwardt F (2008) The P2X7 Carboxyl Tail Is a Regulatory Module of P2X7 Receptor Channel Activity. *J Biol Chem* **283**:25725-25734.
- Braun K, Rettinger J, Ganso M, Kassack M, Hildebrandt C, Ullmann H, Nickel P, Schmalzing G and Lambrecht G (2001) NF449: a Subnanomolar Potency Antagonist at Recombinant Rat P2X1 Receptors. *Naunyn-Schmiedeberg's Arch Pharmacol* **364**:285-290.
- Brotherton-Pleiss CE, Dillon M P, Ford A P, Gever J R, Carter D S, Gleason S K, Lin C J, Moore A G, Thompson A W, Villa M and Zhai Y (2010) Discovery and Optimization of RO-85, a Novel Drug-Like, Potent, and Selective P2X3 Receptor Antagonist. *Bioorg Med Chem Lett* **20**:1031-1036.
- Burnstock G (2004) Introduction: P2 Receptors. *Curr Top Med Chem* **4**:793-803.
- Burnstock G (2008) Purinergic Signalling and Disorders of the Central Nervous System. *Nat Rev Drug Discov* **7**:575-590.
- Cao L, Broomhead H E, Young M T and North R A (2009) Polar Residues in the Second Transmembrane Domain of the Rat P2X2 Receptor That Affect Spontaneous Gating, Unitary Conductance, and Rectification. *J Neurosci* **29**:14257-14264.
- Cockayne DA, Dunn P M, Zhong Y, Rong W, Hamilton S G, Knight G E, Ruan H Z, Ma B, Yip P, Nunn P, McMahon S B, Burnstock G and Ford A P (2005) P2X2 Knockout Mice and P2X2/P2X3 Double Knockout Mice Reveal a Role for the P2X2 Receptor Subunit in Mediating Multiple Sensory Effects of ATP. *J Physiol*.

- Duckwitz W, Hausmann R, Aschrafi A and Schmalzing G (2006) P2X5 Subunit Assembly Requires Scaffolding by the Second Transmembrane Domain and a Conserved Aspartate. *J Biol Chem* **281**:39561-39572.
- Ennion S, Hagan S and Evans R J (2000) The Role of Positively Charged Amino Acids in ATP Recognition by Human P2X1 Receptors. *J Biol Chem* **275**:29361-29367.
- Finger TE, Danilova V, Barrows J, Bartel D L, Vigers A J, Stone L, Hellekant G and Kinnamon S C (2005) ATP Signaling Is Crucial for Communication From Taste Buds to Gustatory Nerves. *Science* **310**:1495-1499.
- Fischer W, Zadori Z, Kullnick Y, Groger-Arndt H, Franke H, Wirkner K, Illes P and Mager P P (2007) Conserved Lysin and Arginin Residues in the Extracellular Loop of P2X3 Receptors Are Involved in Agonist Binding. *Eur J Pharmacol* **576**:7-17.
- Gever JR, Cockayne D A, Dillon M P, Burnstock G and Ford A P (2006) Pharmacology of P2X Channels. *Pflugers Arch* **452**:513-537.
- Gever JR, Soto R, Henningsen R A, Martin R S, Hackos D H, Panicker S, Rubas W, Oglesby I B, Dillon M P, Milla M E, Burnstock G and Ford A P (2010) AF-353, a Novel, Potent and Orally Bioavailable P2X3/P2X2/3 Receptor Antagonist. *Br J Pharmacol* **160**:1387-1398.
- Guerlet G, Taly A, Prado de C L, Martz A, Jiang R, Specht A, Le N N and Grutter T (2008) Comparative Models of P2X2 Receptor Support Inter-Subunit ATP-Binding Sites. *Biochem Biophys Res Commun* **375**:405-409.
- Hausmann R, Rettinger J, Gerevich Z, Meis S, Kassack M U, Illes P, Lambrecht G and Schmalzing G (2006) The Suramin Analog 4,4',4'',4'''-(Carbonylbis(Imino-5,1,3-Benzenetriylbis (Carbonylimino)))Tetra-Kis-Benzenesulfonic Acid (NF110) Potently Blocks P2X3 Receptors: Subtype Selectivity Is Determined by Location of Sulfonic Acid Groups. *Mol Pharmacol* **69**:2058-2067.

- Henikoff S and Henikoff J G (1992) Amino Acid Substitution Matrices From Protein Blocks. *Proc Natl Acad Sci U S A* **89**:10915-10919.
- Jahangir A, Alam M, Carter D S, Dillon M P, Bois D J, Ford A P, Gever J R, Lin C, Wagner P J, Zhai Y and Zira J (2009) Identification and SAR of Novel Diaminopyrimidines. Part 2: The Discovery of RO-51, a Potent and Selective, Dual P2X3/P2X2/3 Antagonist for the Treatment of Pain. *Bioorg Med Chem Lett* **19**:1632-1635.
- Jarvis MF (2010) The Neural-Glial Purinergic Receptor Ensemble in Chronic Pain States. *Trends Neurosci* **33**:48-57.
- Jarvis MF, Burgard E C, McGaraughty S, Honore P, Lynch K, Brennan T J, Subieta A, van Biesen T, Cartmell J, Bianchi B, Niforatos W, Kage K, Yu H, Mikusa J, Wismer C T, Zhu C Z, Chu K, Lee C H, Stewart A O, Polakowski J, Cox B F, Kowaluk E, Williams M, Sullivan J and Faltynek C (2002) A-317491, a Novel Potent and Selective Non-Nucleotide Antagonist of P2X3 and P2X2/3 Receptors, Reduces Chronic Inflammatory and Neuropathic Pain in the Rat. *Proc Natl Acad Sci U S A* **99**:17179-17184.
- Jarvis MF and Khakh B S (2009) ATP-Gated P2X Cation-Channels. *Neuropharmacology* **56**:208-215.
- Jiang R, Martz A, Gonin S, Taly A, de Carvalho L P and Grutter T (2010) A Putative Extracellular Salt Bridge at the Subunit Interface Contributes to the Ion Channel Function of the ATP-Gated P2X2 Receptor. *J Biol Chem* **285**:15805-15815.
- Kassack MU, Braun K, Ganso M, Ullmann H, Nickel P, Boing B, Muller G and Lambrecht G (2004) Structure-Activity Relationships of Analogues of NF449 Confirm NF449 As the Most Potent and Selective Known P2X1 Receptor Antagonist. *Eur J Med Chem* **39**:345-357.
- Kawate T, Michel J C, Birdsong W T and Gouaux E (2009) Crystal Structure of the ATP-Gated P2X4 Ion Channel in the Closed State. *Nature* **460**:592-598.

- Keceli B and Kubo Y (2009) Functional and Structural Identification of Amino Acid Residues of the P2X2 Receptor Channel Critical for the Voltage- and [ATP]-Dependent Gating. *J Physiol* **587**:5801-5818.
- Khakh BS, Gittermann D, Cockayne D A and Jones A (2003) ATP Modulation of Excitatory Synapses Onto Interneurons. *J Neurosci* **23**:7426-7437.
- Kracun S, Chaptal V, Abramson J and Khakh B S (2010) Gated Access to the Pore of a P2X Receptor: Structural Implications for Closed-Open Transitions. *J Biol Chem*.
- Labute P (2008) The Generalized Born/Volume Integral Implicit Solvent Model: Estimation of the Free Energy of Hydration Using London Dispersion Instead of Atomic Surface Area. *J Comput Chem* **29**:1693-1698.
- Labute P (2009) Protonate3D: Assignment of Ionization States and Hydrogen Coordinates to Macromolecular Structures. *Proteins* **75**:187-205.
- Needleman SB and Wunsch C D (1970) A General Method Applicable to the Search for Similarities in the Amino Acid Sequence of Two Proteins. *J Mol Biol* **48**:443-453.
- Nicke A, Bäumer H G, Rettinger J, Eichele A, Lambrecht G, Mutschler E and Schmalzing G (1998) P2X1 and P2X3 Receptors Form Stable Trimers: a Novel Structural Motif of Ligand-Gated Ion Channels. *EMBO J* **17**:3016-3028.
- Rettinger J, Braun K, Hochmann H, Kassack M U, Ullmann H, Nickel P, Schmalzing G and Lambrecht G (2005) Profiling at Recombinant Homomeric and Heteromeric Rat P2X Receptors Identifies the Suramin Analogue NF449 As a Highly Potent P2X1 Receptor Antagonist. *Neuropharmacology* **48**:461-468.
- Roberts JA, Digby H R, Kara M, El A S, Sutcliffe M J and Evans R J (2008) Cysteine Substitution Mutagenesis and the Effects of Methanethiosulfonate Reagents at P2X2 and P2X4 Receptors Support a Core Common Mode of ATP Action at P2X Receptors. *J Biol Chem* **283**:20126-20136.

- Roberts JA and Evans R J (2004) ATP Binding at Human P2X1 Receptors. Contribution of Aromatic and Basic Amino Acids Revealed Using Mutagenesis and Partial Agonists. *J Biol Chem* **279**:9043-9055.
- Rong W, Gourine A V, Cockayne D A, Xiang Z, Ford A P, Spyer K M and Burnstock G (2003) Pivotal Role of Nucleotide P2X2 Receptor Subunit of the ATP-Gated Ion Channel Mediating Ventilatory Responses to Hypoxia. *J Neurosci* **23**:11315-11321.
- Summa CM and Levitt M (2007) Near-Native Structure Refinement Using in Vacuo Energy Minimization. *Proc Natl Acad Sci U S A* **104**:3177-3182.
- Surprenant A and North R A (2009) Signaling at Purinergic P2X Receptors. *Annu Rev Physiol* **71**:333-359.
- Trujillo CA, Nery A A, Martins A H, Majumder P, Gonzalez F A and Ulrich H (2006) Inhibition Mechanism of the Recombinant Rat P2X(2) Receptor in Glial Cells by Suramin and TNP-ATP. *Biochemistry* **45**:224-233.
- Ullmann H, Meis S, Hongwiset D, Marzian C, Wiese M, Nickel P, Communi D, Boeynaems J M, Wolf C, Hausmann R, Schmalzing G and Kassack M U (2005) Synthesis and Structure-Activity Relationships of Suramin-Derived P2Y11 Receptor Antagonists With Nanomolar Potency. *J Med Chem* **48**:7040-7048.
- Wilkinson WJ, Jiang L H, Surprenant A and North R A (2006) Role of Ectodomain Lysines in the Subunits of the Heteromeric P2X2/3 Receptor. *Mol Pharmacol* **70**:1159-1163.

Footnotes

This research project is supported by grants of the Deutsche Forschungsgemeinschaft to G.S. (Schm 536/8-1/2) and R.H. (Schm 536/8-2) and M.U.K. (Graduiertenkolleg GRK677).

¹ C.W. and C.R., Equal contribution

Legends to figures

Fig. 1. *Potencies of NF770, NF776 and NF778 at different rP2X receptor isoforms.* (A) Steady-state protocol for the assessment of the inhibitory potency of NF770 from stationary current measurements. A representative original current trace is shown. After a maximal stationary current (max) was elicited with 10 μ M ATP (light gray), 30 nM NF770 was co-applied with 10 μ M ATP (dark gray). The current declined until a new steady state was reached, designated the minimum current (min), indicating that inhibition by NF770 was fully developed. The application of ATP and NF770 was then terminated. The extent of inhibition was judged from the ratio of the maximal and minimal stationary current in the absence and presence of NF770, respectively. (B) Traces representing the protocol for the assessment of the inhibitory potency of NF770 from peak current measurements. Representative original current traces are shown. rP2X1 receptor-expressing oocytes were repetitively activated with 1 μ M ATP (light gray) at 1-min intervals. Between two control measurements, the oocytes were pre-equilibrated with 300 nM NF770 for 30 s (hatched gray) and then challenged with 1 μ M ATP in the continued presence of NF770 (dark gray). The extent of inhibition was judged from the reduction of the peak current amplitude compared with the two flanking control measurements. (C-E) Using the appropriate steady-state or peak-current protocol, concentration-inhibition curves were generated in the presence of incrementally larger concentrations of (C) NF770, (D) NF776, (E) NF778. For convenience, all IC₅₀ values of NF770, NF776 and NF778 are summarized in Table 1, and the chemical structures are shown in Table 2.

Fig. 2. *Assessment of the mechanism of NF770-induced inhibition of the rP2X2 receptor.* (A) Representative original current traces are shown. Oocytes expressing rP2X2 receptors were repetitively activated with indicated increasing concentrations of ATP in the absence (light

gray) or the presence of 3 μM NF770 (dark grey), respectively. (B) ATP concentration–response curves were established by stimulating oocytes expressing the rP2X2 receptor with incrementally larger concentrations of ATP in the absence of NF770 (■, $\text{EC}_{50} = 20.7 \mu\text{M}$ (18.9 - 22.7) and $n_{\text{H}} = 1.7 \pm 0.1$, $n = 11$) or the presence of 30 nM NF770 (▲, $\text{EC}_{50} = 28.7 \mu\text{M}$ (23.2 - 35.6) and $n_{\text{H}} = 1.4 \pm 0.2$, $n = 5$), 300 nM NF770 (▼, $\text{EC}_{50} = 67.9 \mu\text{M}$ (47.4 - 97.1) and $n_{\text{H}} = 0.9 \pm 0.1$, $n = 6$), 1 μM NF770 (◆, $\text{EC}_{50} = 116.1 \mu\text{M}$ (78.1 - 172.4) and $n_{\text{H}} = 1.0 \pm 0.1$, $n = 6$) and 3 μM NF770 (●, $\text{EC}_{50} = 279.5 \mu\text{M}$ (183.0 – 426.8) and $n_{\text{H}} = 1.0 \pm 0.1$, $n = 5$). Currents were normalized to those elicited by a supersaturating concentration of ATP (1 mM). (C) Schild plot analysis of the data from (A) yielded a regression slope of 0.74 ± 0.03 and a pA_2 value of 6.96 (negative x-axis intercept). Linear regression analysis shows no significant deviation from linearity ($r^2=0.996$). The dotted grey line indicates a regression slope of 1.

Fig. 3. *Homology model of the rP2X2 with NF770 and related compounds bound within the modeled ATP-binding pocket.* (A) Stereoview of the homology-modeled homotrimeric rP2X2 receptor structure with the docked NF770 as viewed from the side i.e., parallel to the membrane plane. One of a total of three ATP-binding sites located between neighboring subunits is highlighted with one NF770 molecule bound. β -sheets are depicted in yellow, α -helical structures in red and random coil regions in cyan. The gray bars mark the presumed boundaries of the outer (out) and inner (in) leaflets of the membrane bilayer. The ATP-binding pocket consists primarily of hydrophilic residues (indicated in pink), suggesting that polar substituents of the ligand are involved in strong binding. Neutral and hydrophobic residues are indicated in white and green, respectively.

Inset: Close-up view of the docking of NF770 into the ATP-binding pocket. One NF770 molecule (shown in stick representation) interacts with residues of two adjacent subunits

(colored in green and red) that form the ATP-binding pocket. The binding pocket is large enough to accommodate the entire large urea derivative NF770, thus allowing NF770 to interact with residues deep within the ATP-binding pocket and in the outer sphere. Specific atoms of NF770 are colored by element type: carbons and hydrogens (dark gray), sulfur (yellow), oxygen (red) and nitrogen (dark blue). The planar structure of NF770 is shown at the bottom. (B) Comparison of the binding modes of NF770, NF769 and NF742. The suramin derivatives NF770 (pink), NF769 (gray) and NF742 (orange) in their lowest-energy conformations are superimposed within the rP2X2 receptor binding pocket as obtained by docking to our homology model. Selected residues of the rP2X2 receptor binding site are shown as green sticks, while the side chains of Gly72 and Arg290 are shown as balls and sticks. Specific atoms of the ligands are colored as detailed in A. NF770 and NF769, which both carry the naphthalene moiety in the 7,7' position relative to the amine group, are directed by a Gly72–sulfonate group interaction to orient spatially so that their methoxy group comes into close apposition to Arg290. As a result, a hydrogen bond can be formed that, according to our modeling data, is a key determinant of the interaction of NF769 and NF770 with the rP2X2 receptor. The close distance of 2.13 Å between the methoxy group and Arg290 (yellow bar) seems to account for the stronger binding and higher potency of NF770 compared to NF769, the methoxy group of which is 3.69 Å from Arg290 (yellow bar). NF742 lacks this interaction and partially protrudes from the binding pocket because its 8,8' positioned naphthalene moiety is conformationally less flexible than that of NF770 and NF769. As a result, NF742 is a much weaker blocker of the rP2X2 receptor ($IC_{50} > 20 \mu M$) than NF770 (IC_{50} 19 nM). (C) 2D interaction plot of NF770 within the rP2X2 binding pocket. The molecular contacts between the ATP-binding pocket formed by two subunits (A and B) and NF770, as derived from our homology model and the identified binding mode of the ligand, are shown. Interacting residues are designated with letters A and B to indicate subunits A and

B, respectively. Corresponding 2D plots of NF769 and NF742 within the binding pocket are shown in (Supplemental Figure 1A,B).

Fig. 4. Effect of mutation of Gly72, Glu167 or Arg290 of the rP2X2 receptors on ATP potency. (A) Representative original current traces elicited by 1 mM ATP (gray area) of the indicated wild-type or mutant rP2X2 receptors demonstrate that the non-desensitizing behavior is unchanged, while the maximal current amplitudes are altered. (B) ATP concentration–response curves. Absolute current amplitudes are indicated. Red ■ wt-rP2X2, $EC_{50} = 18.5$ (14.5-23.6) μM and $n_H = 1.4 \pm 0.2$, $n = 12$; ▼ $G^{72}\text{A}$ -rP2X2, $EC_{50} = 243.6$ (212.1-271.3) μM and $n_H = 1.5 \pm 0.4$, $n = 8$; ▲ $R^{290}\text{A}$ -rP2X2., $EC_{50} = 504.8$ (412.3-603.1) μM and $n_H = 1.6 \pm 0.7$, $n = 8$; ● $E^{167}\text{A}$ -rP2X2, $EC_{50} = 3.6$ (2.7-4.9) μM and $n_H = 1.4 \pm 0.2$, $n = 8$. (C) [^{35}S]Methionine-labeled oocytes were chased for 24 h and surface-labeled with the membrane-impermeant fluorescent Cy5 dye prior to protein purification by Ni-NTA chromatography. Samples were resolved by reducing SDS-urea-PAGE and visualized in their Cy5-labeled surface form by Typhoon fluorescence scanning. Numbers in left margin indicate the molecular masses in kDa of the marker proteins.

Table 1. Survey of the potencies of NF770, NF776 and NF778 at various recombinant P2X receptors. IC₅₀ values represent data from 5–7 separate experiments.

	NF770			NF776			NF778		
	- log IC ₅₀ (95% CI) ^a	IC ₅₀ (nM)	Normalized IC ₅₀ ^b	- log IC ₅₀ (95% CI) ^a	IC ₅₀ (nM)	Normalized IC ₅₀ ^c	- log IC ₅₀ (95% CI) ^a	IC ₅₀ (nM)	Normalized IC ₅₀ ^d
wt-rP2X1	6.03 (6.20-5.86)	939	49.4	n.d. ^e	n.d. ^e	-	n.d. ^e	n.d. ^e	-
rP2X2-X1	6.60 (6.76-6.44)	251	13.2	6.40 (6.52-6.27)	400	4.1	6.38 (6.47-6.29)	415	3.0
wt-rP2X2	7.73 (7.79-7.67)	19	1	7.01 (7.08-6.94)	97	1	6.86 (6.92-6.79)	140	1
wt-rP2X3	7.13 (7.21-7.05)	74	3.9	n.d. ^e	n.d. ^e	-	n.d. ^e	n.d. ^e	-
rP2X2-X3	7.65 (7.69-7.60)	23	1.2	6.07 (6.14-5.99)	861	8.9	6.18 (6.31-6.06)	655	4.7
wt-P2X2/3	7.38 (7.44-7.33)	41	2.2	6.96 (7.02-6.89)	111	1.1	6.16 (6.23-6.08)	698	5.0
wt-rP2X4	> 5	> 10,000	-	> 5	> 10,000	-	> 5	> 10,000	-
wt-rP2X7	> 5	> 10,000	-	> 5	> 10,000	-	> 5	> 10,000	-

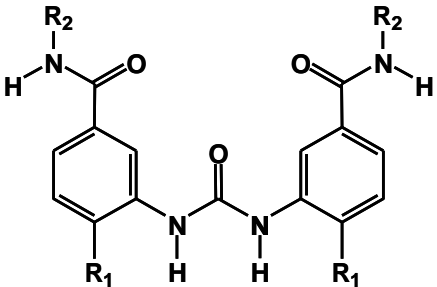
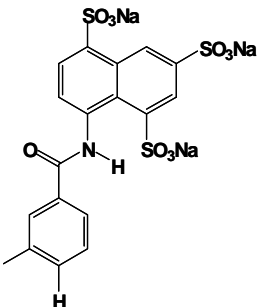
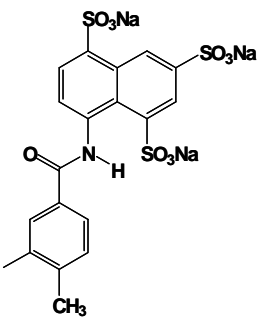
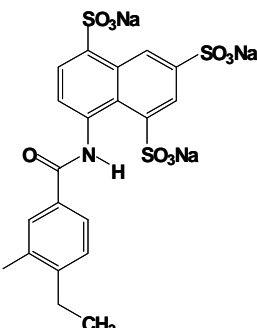
^a 95% Confidence Interval

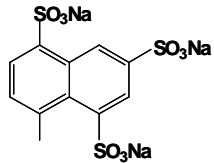
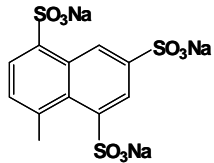
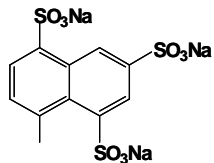
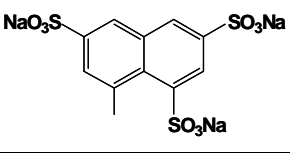
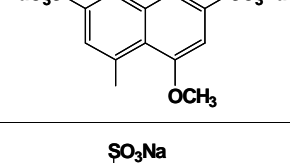
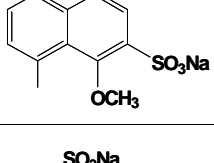
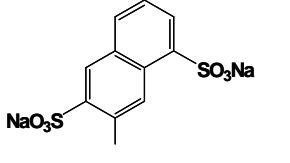
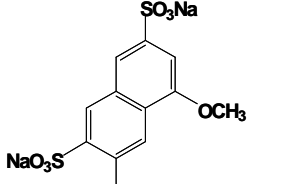
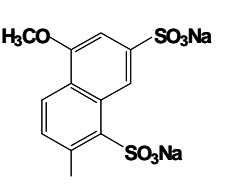
^{b,c,d} Normalized to the following the IC₅₀ values for rP2X2 receptor inhibition: ^b 19 nM NF770, ^c 97 nM NF776, ^d 140 nM NF778

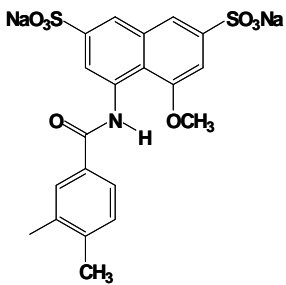
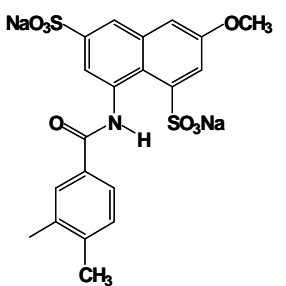
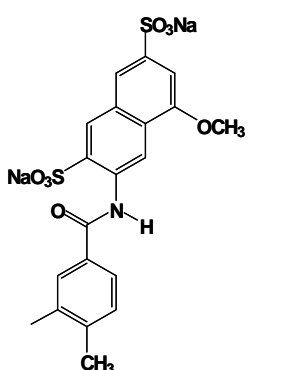
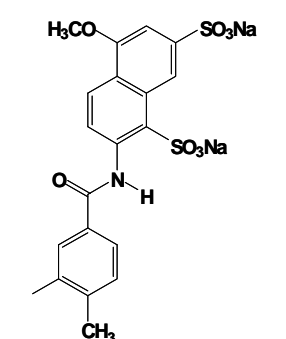
^e Not determined

Table 2

Table 2. Chemical structures of suramin derivatives and their IC_{50} values at the $rP2X_2$ receptor. IC_{50} values were derived from concentration–inhibition curves established with the steady-state protocol detailed in Fig. 1A.

			
Compound (Derivative ^a)	R ₁	R ₂	IC ₅₀ (μM) (95% CI ^b)
1 (NF037)	H		0.28 (0.22-0.35)
2 (Suramin)	H		0.49 (0.47-0.52)
3 (NF127)	H		0.32 (0.29-0.36)

4 (NF023)	H		12.9 (5.9-27.7)
5 (NF058)	CH₃		14.4 (7.7-26.9)
6 (NF124)	CH₂-CH₃		9.9 (5.8-16.7)
7 (NF248)	CH₃		22.8 (14.2-28.4)
8 (NF739)	CH₃		5.1 (4.5-5.7)
9 (NF755)	CH₃		10.9 (3.6-22.1)
10 (NF252)	CH₃		4.6 (1.1-8.7)
11 (NF769)	CH₃		1.3 (1.1-1.4)
12 (NF776)	CH₃		0.097 (0.084-0.114)

13 (NF742)	H		22.1 (14.1-27.1)
14 (NF763)	H		0.65 (0.39-1.11)
15 (NF770)	H		0.019 (0.016-0.022)
16 (NF778)	H		0.14 (0.121-0.161)

^a For suramin derivatives that have been described in previous papers or analyzed in detail in the present study, the corresponding generic name is given.

^b 95% Confidence Interval

Generic names of compounds: NF037, 8,8'-(Carbonylbis(imino-3,1-phenylenecarbonylimino-3,1-phenylenecarbonylimino))bis(naphthalene-1,3,5-trisulfonic acid) hexasodium salt;

Suramin, 8,8'-(Carbonylbis(imino-3,1-phenylenecarbonylimino-3,1-(4-methylphenylene)carbonylimino))bis(naphthalene-1,3,5-trisulfonic acid) hexasodium salt; NF127, 8,8'-(Carbonylbis(imino-3,1-phenylenecarbonylimino-3,1-(4-ethylphenylene)carbonylimino))bis(naphthalene-1,3,5-trisulfonic acid) hexasodium salt; NF023, 8,8'-(Carbonylbis(imino-3,1-phenylenecarbonylimino))bis(naphthalene-1,3,5-trisulfonic acid) hexasodium salt; NF058, 8,8'-(Carbonylbis(imino-3,1-(4-methylphenylene)carbonylimino))bis(naphthalene-1,3,5-trisulfonic acid) hexasodium salt; NF124, 8,8'-(Carbonylbis(imino-3,1-(4-ethylphenylene)carbonylimino))bis(naphthalene-1,3,5-trisulfonic acid) hexasodium salt; NF248, 8,8'-(Carbonylbis(imino-3,1-(4-methylphenylene)carbonylimino))bis(naphthalene-1,3,6-trisulfonic acid) hexasodium salt; NF739, 8,8'-(Carbonylbis(imino-3,1-(4-methylphenylene)carbonylimino))bis(1-methoxynaphthalene-3,6-disulfonic acid) tetrasodium salt; NF755, 8,8'-(Carbonylbis(imino-3,1-(4-methylphenylene)carbonylimino))bis(1-methoxynaphthalene-2,5-disulfonic acid) tetrasodium salt; NF252, 7,7'-(Carbonylbis(imino-3,1-(4-methylphenylene)carbonylimino))bis(naphthalene-1,3,6-trisulfonic acid) hexasodium salt; NF769, 7,7'-(Carbonylbis(imino-3,1-(4-methylphenylene)carbonylimino))bis(1-methoxynaphthalene-3,6-disulfonic acid) tetrasodium salt; NF776, 6,6'-(Carbonylbis(imino-3,1-(4-methylphenylene)carbonylimino))bis(1-methoxynaphthalene-3,5-disulfonic acid) tetrasodium salt; NF742, 8,8'-(Carbonylbis(imino-3,1-phenylenecarbonylimino-3,1-(4-methylphenylene)carbonylimino))bis(1-methoxynaphthalene-3,6-disulfonic acid) tetrasodium salt; NF763, 8,8'-(Carbonylbis(imino-3,1-phenylenecarbonylimino-3,1-(4-methylphenylene)carbonylimino))bis(3-methoxynaphthalene-1,6-disulfonic acid) tetrasodium salt; NF770, 7,7'-(Carbonylbis(imino-3,1-phenylenecarbonylimino-3,1-(4-methylphenylene)carbonylimino))bis(1-methoxynaphthalene-3,6-disulfonic acid) tetrasodium salt; NF778, 6,6'-(Carbonylbis(imino-3,1-phenylenecarbonylimino-3,1-(4-methylphenylene)carbonylimino))bis(1-methoxynaphthalene-3,5-disulfonic acid) tetrasodium salt.

Fig. 1

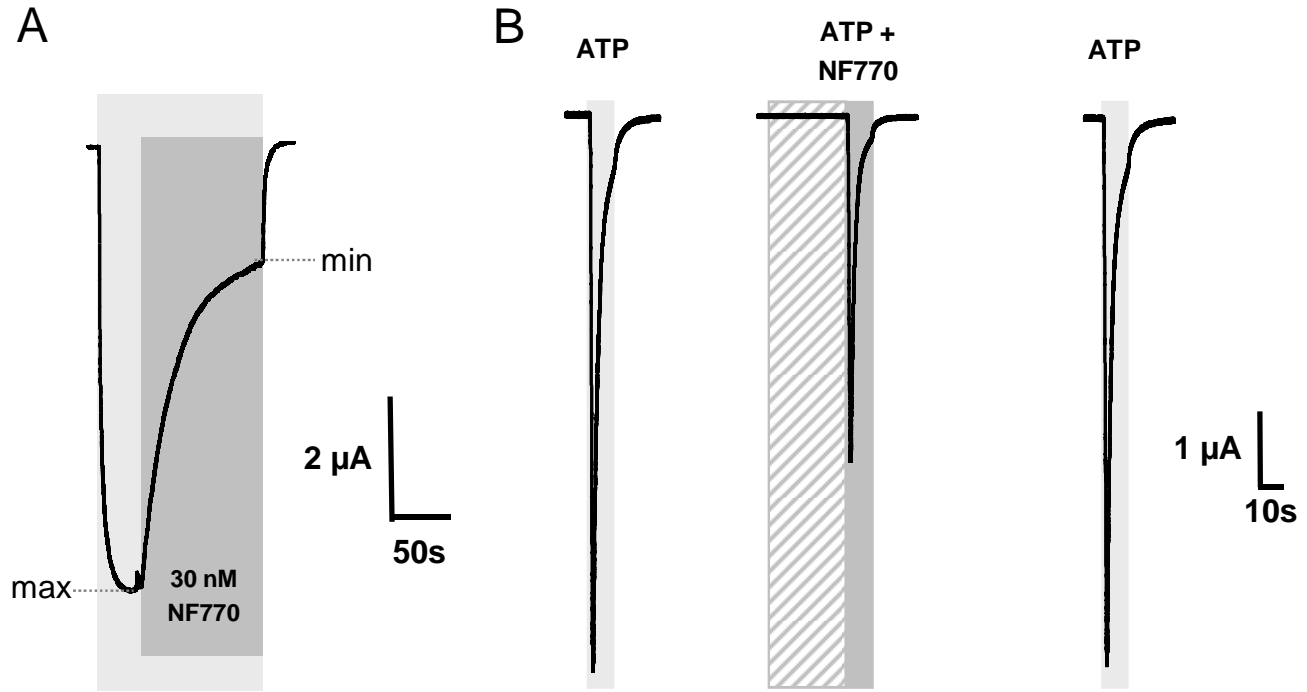
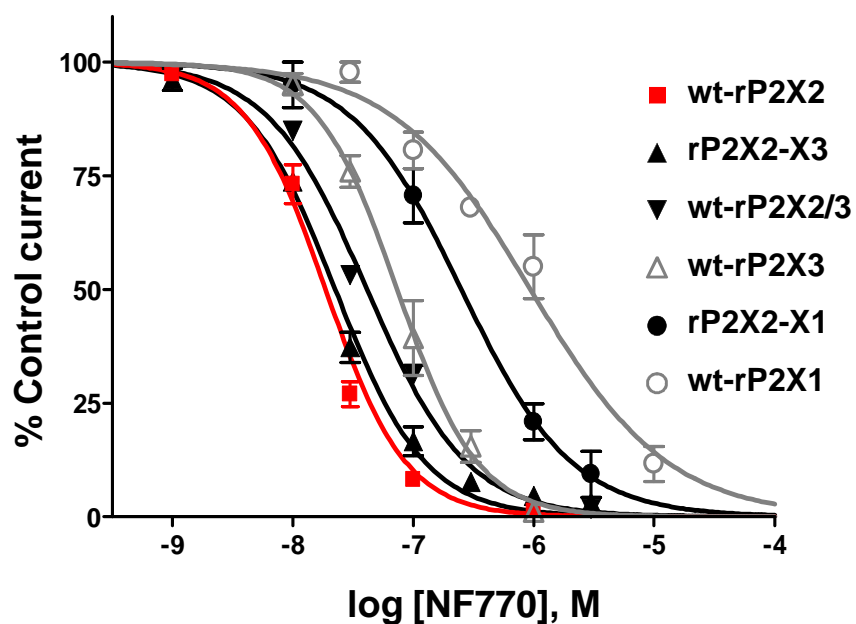
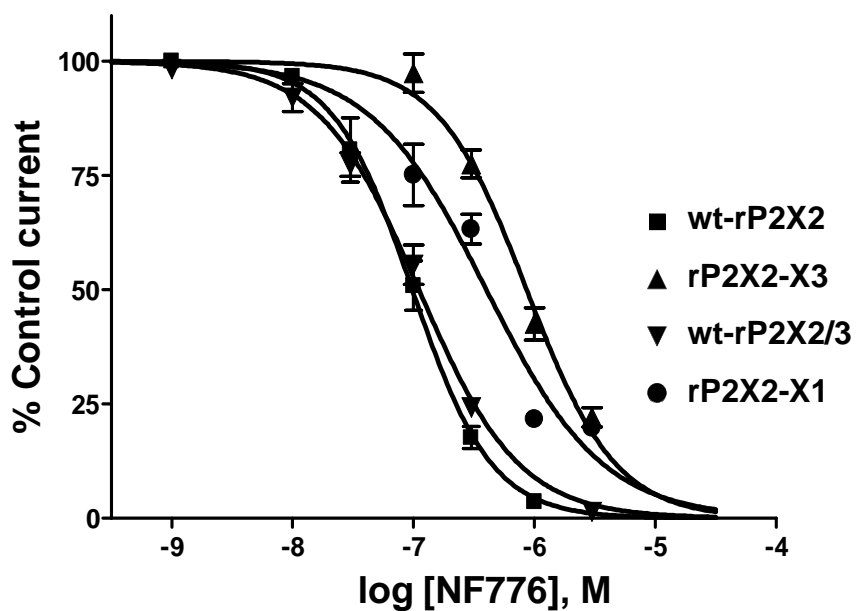


Fig. 1

C



D



E

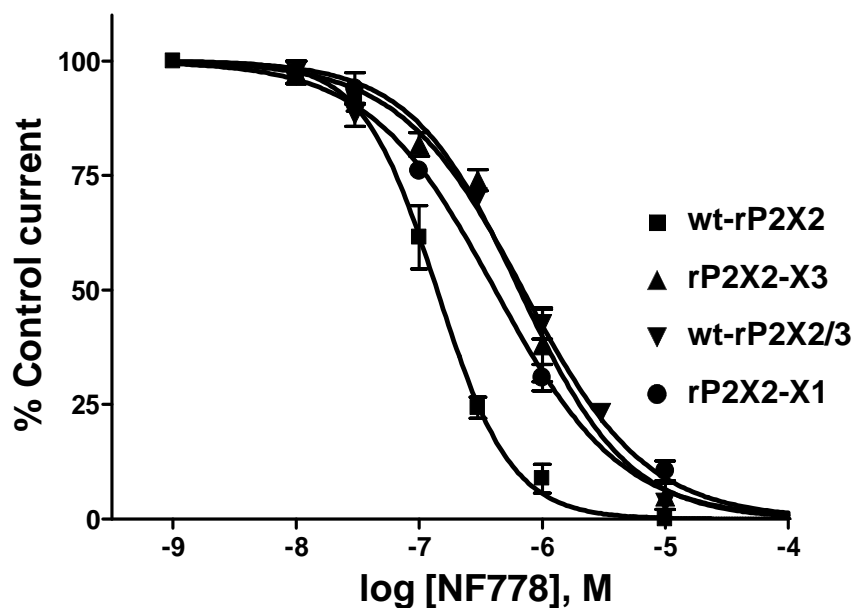
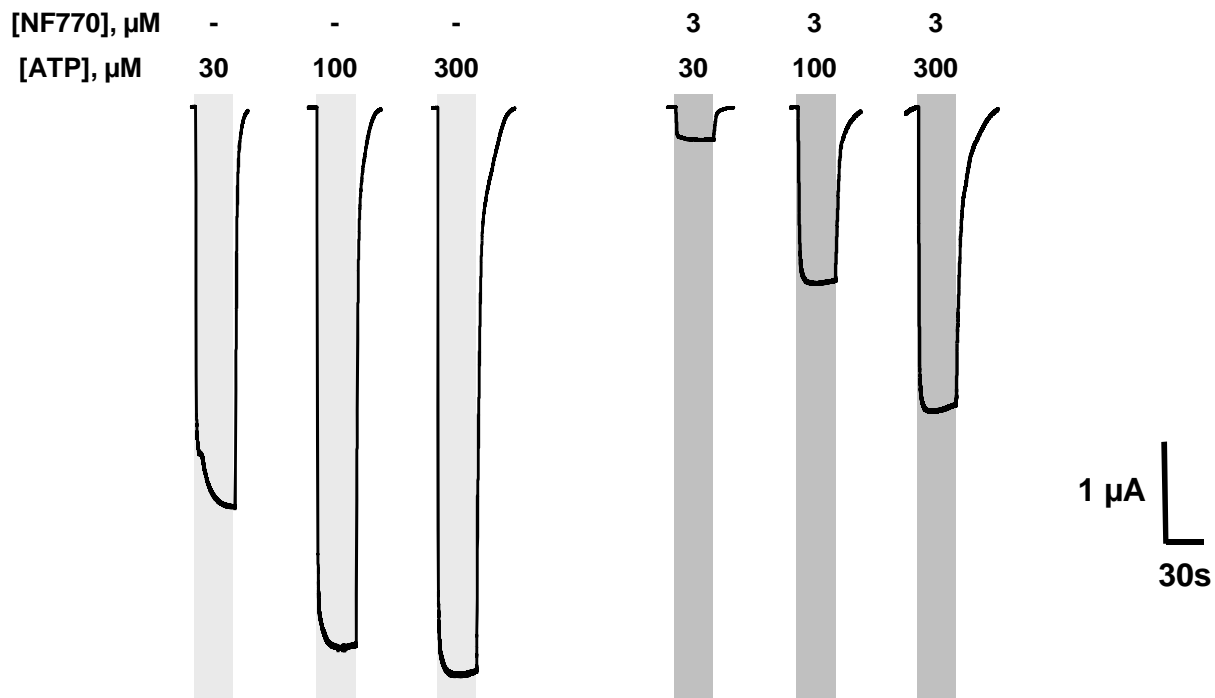
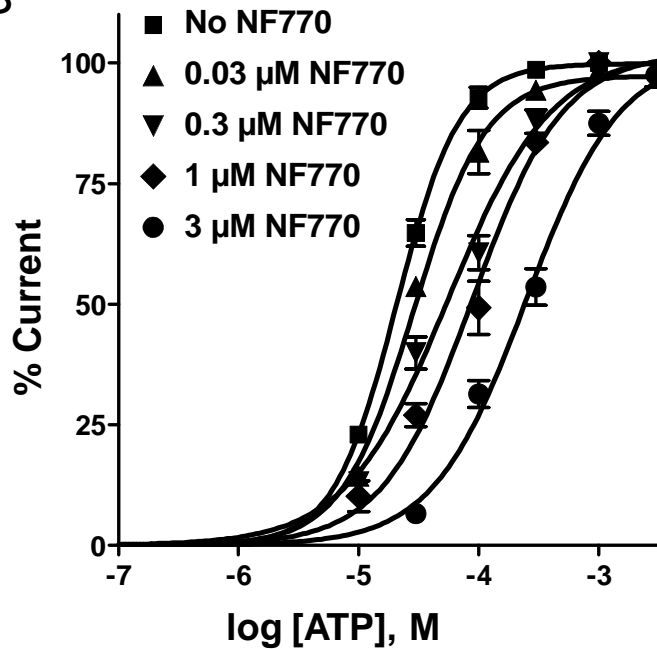


Fig. 2

A



B



C

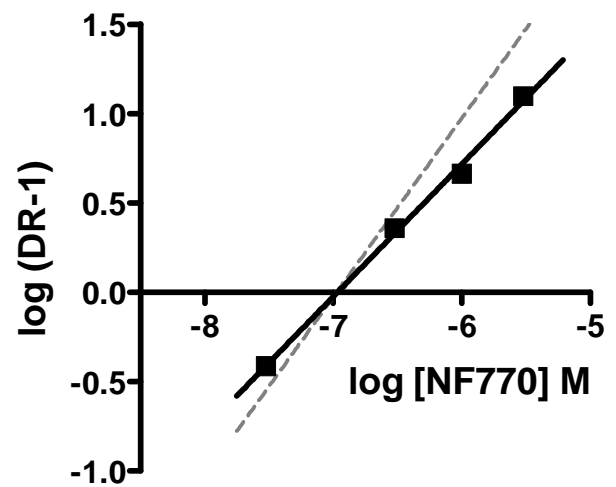


Fig. 3

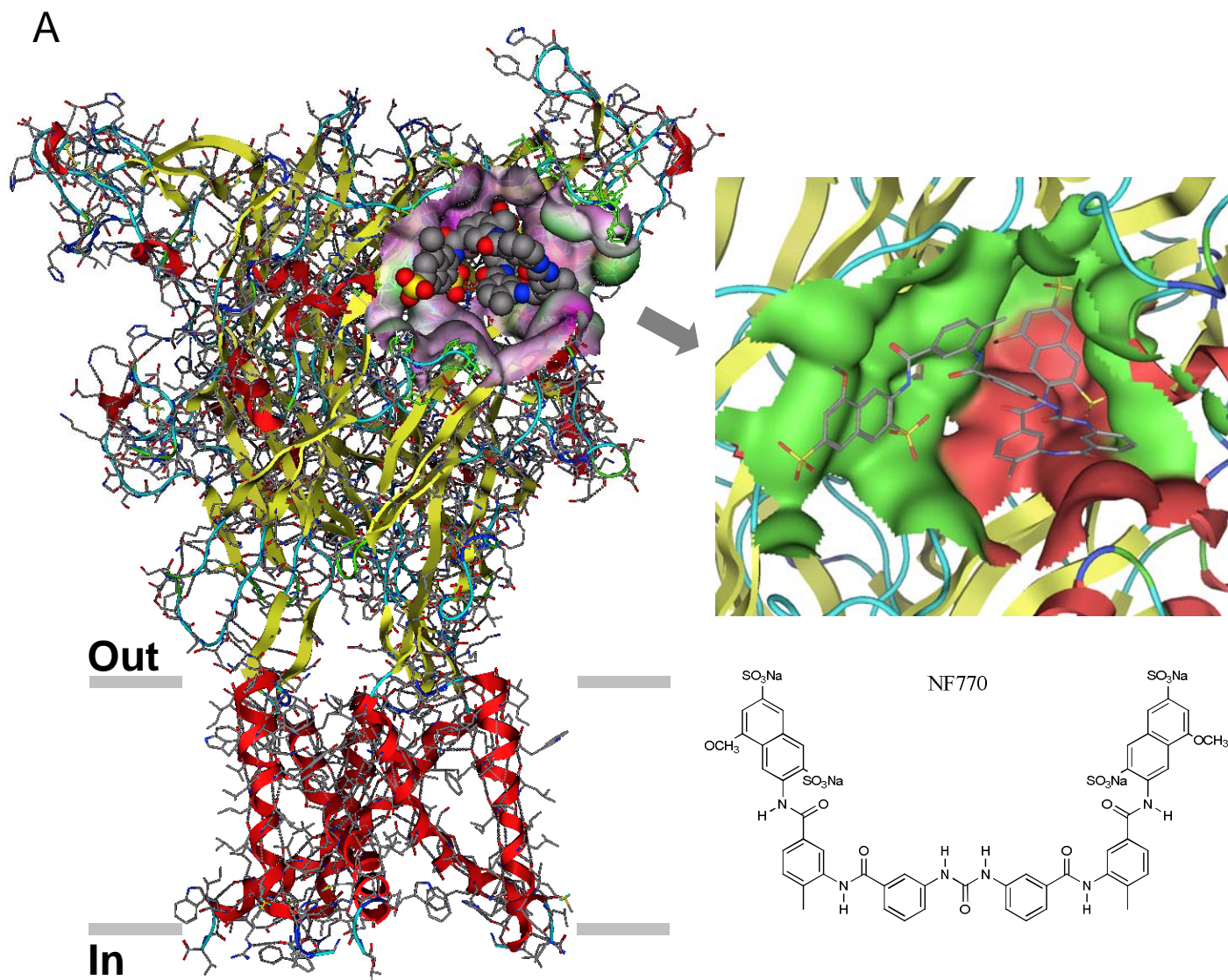


Fig. 3

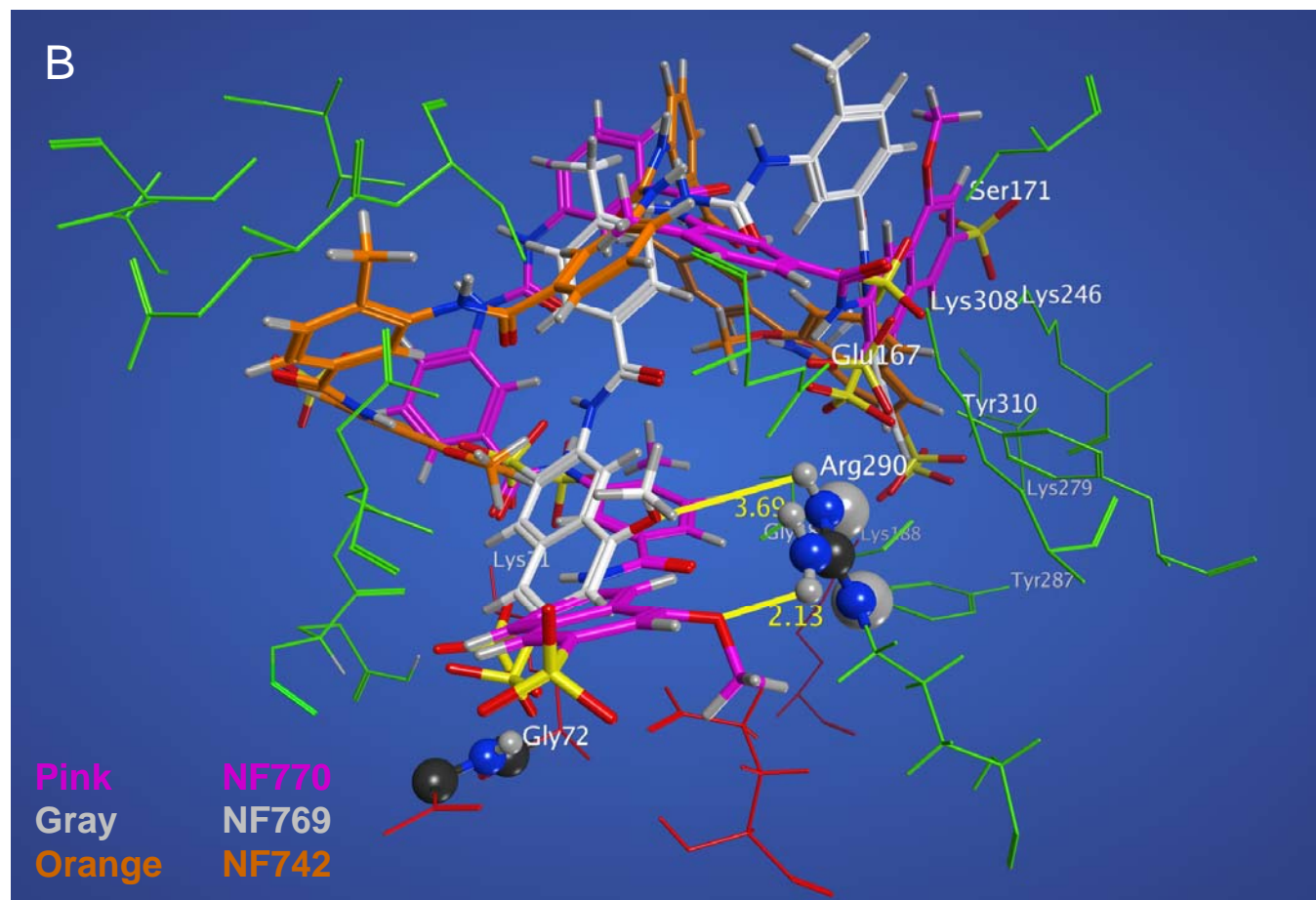


Fig. 3

C

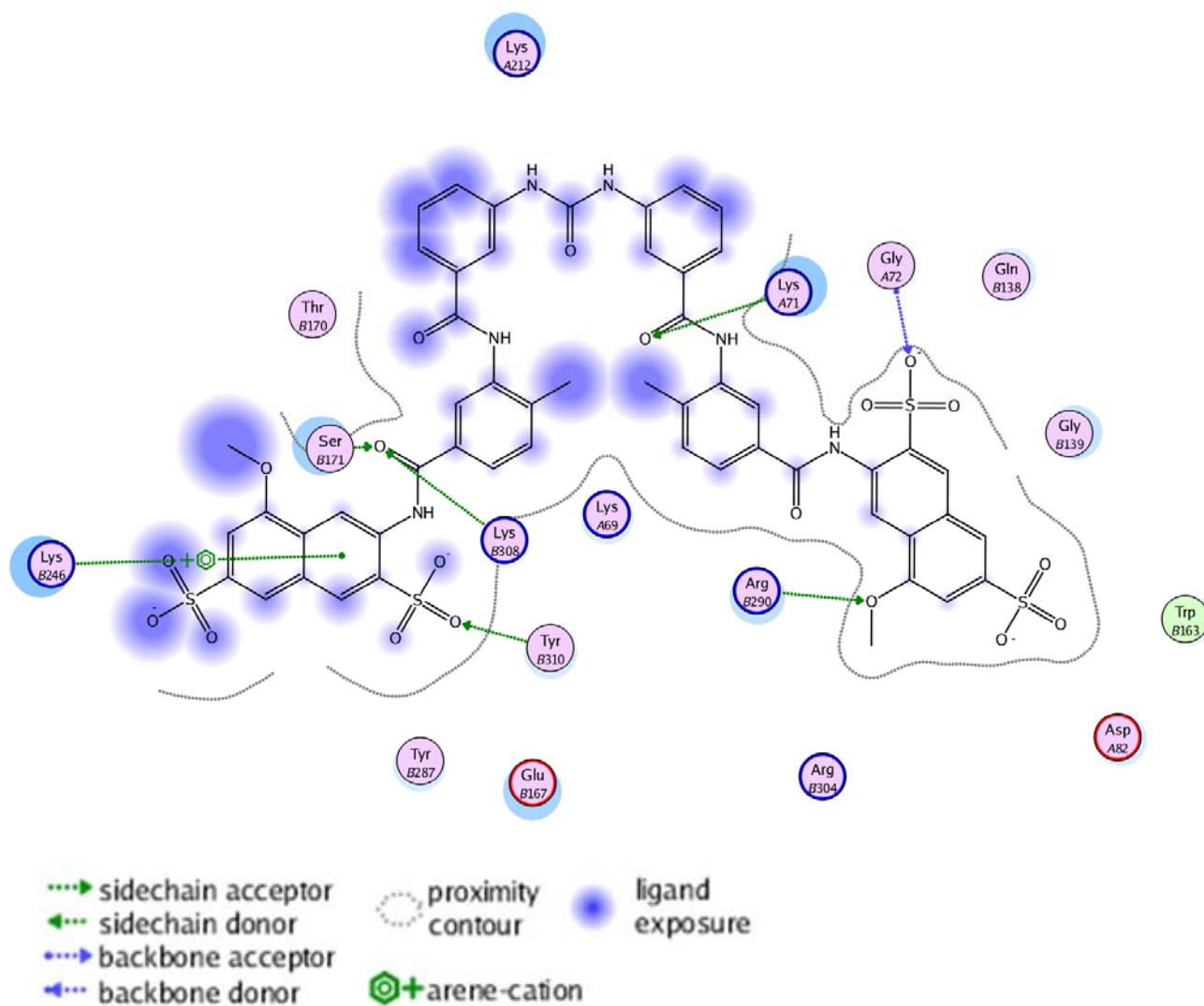


Fig. 4

